energies

MDPI

Article

Solar Concentrator Consisting of Multiple Aspheric Reflectors

Guobin Cao [1], Hua Qin [2,*], Rajan Ramachandran [2] and Bo Liu [2,*]

[1] Beijing Railway Century Soil Engineering Co., LTD, Yangfangdian Road, Haidian District, Beijing 100038, China; baiducgb@gmail.com

[2] Laboratory of Functional Molecules and Materials, School of Physics and Optoelectronic Engineering, Shandong University of Technology, Zibo, Shandong 255000, China; ramu.rasan@gmail.com

* Correspondence: zfjqinh@163.com (H.Q.); liub@sdut.edu.cn (B.L.); Tel.: +05-33-2783909 (H.Q. & B.L.)

Received: 30 September 2019; Accepted: 22 October 2019; Published: 23 October 2019

Abstract: This paper presents an off-axis-focused solar concentrator system consisting of 190 aspheric reflectors, where the aperture radius of each reflector is 10 cm, and vertices of all reflectors are orderly arranged in the same plane. The aspheric parameters controlling the curvature of the reflectors are determined using coordinate transformations and the particle swarm optimization (PSO) algorithm. Based on these aspheric parameters, the light distribution of focal plane was calculated by the ray tracing method. The analyses show that the designed concentrator system has a spot radius of less than 1 cm and the concentration ratio over 3300:1 is achieved using only one reflection. The design results have been verified with the optical design software Zemax.

Keywords: concentrating solar power system; aspheric reflector; off-axis point focusing; PSO algorithm

1. Introduction

Solar energy is often considered as one of the most viable renewable energy sources because it is unpolluted, abundant, and holds great promises for utilization and sustainable development in the near future [1,2]. Solar thermal and photovoltaic (PV) power generations are the two major applications of solar energy currently in use. In the case of solar thermal power generation, steam is generated and then current is produced using the steam turbine, whereas in the case of solar PV power generation, solar radiation is directly converted into the electricity [3–5]. Use of solar concentrator is an effective approach in solar PV power generation in order to increase the output power and to reduce the investment cost [6].

In the last five decades, various forms of devices making use of solar concentrators to heat a heat transfer medium or working fluid were developed providing power to mechanical equipment. The models of the concentrators can be cataloged into parabolic dishes [7,8], Fresnel lenses [9,10], parabolic troughs [11], special bowls [12], etc. For example, a parabolic dish concentrator is mounted using sun-tracking mechanism and its motion is well controlled. The solar radiation is focused on the thermal receiver placed at the focal point. A trough concentrator is a solar linear focusing device, and the solar radiation is focused on tubular heat absorbers placed along its focal line. A trough concentrator could produce a temperature of about 100 °C, and dish systems could reach a concentration temperature of 1500 °C at the receiver [13]. The sunlight concentration ratio must be improved in order to increase the focusing temperature. The theoretical concentration ratio for trough solar concentrators and dish concentrators were 285:1 [14] and 2240:1 [15,16], respectively. At present, the concentration ratio for a large trough solar concentrator made in domestic enterprises is generally up to 80:1 and for a large dish solar concentrator, it is usually about 1000:1.

Most of the important developments of solar concentrators have been done in the solar thermal and PV systems. In the solar thermal system, the most common method is to increase focusing stages and reflectors. Rodriguez-Sanchez et al. (2015) employed secondary devices to optimize the focusing position and the incidence angle of sunlight [17]. Balaji et al. (2016) employed the combination of multi-stage focusing and multiple reflectors to increase the concentration ratio and also to improve the flux distribution over the circumference of the absorber [18]. Benyakhlef et al. (2016) used multiple rotating curved heliostats instead of flat ones to reflect the sun-rays onto the linear receiver at a fixed position. Primary focusing heliostats were arranged in rows whereas the secondary reflector was only one reflector. Interestingly, the curvature allowed the heliostats to be more precise than in flat ones and offered a higher concentration capacity [19]. Sharma et al. (2015) utilized the line Fresnel reflector (LFR) field consisting of parallel rows of collectors in which each collector-row was composed of parallel rows of reflectors that direct the sun-rays toward linear receivers [20]. Qin et al. (2013) raised the concentration ratio of a trough concentrator to 285:1 in case of off-axis focus by adopting reflective aspheric surfaces [14]. Recently, a prototype of two-stage non-imaging solar concentrator showed a higher concentration ratio at the receiver plane [21]. However, improving the spatial uniformity can efficiently increase the concentration ratio. A new concept of high-flux non-coaxial concentrating solar simulator was introduced to the typical ellipsoidal reflectors [22]. In some cases, multiple reflectors were used to focus the solar beam on the same small area in order to increase the temperature of the focus area [23–26]. Loni et al. (2016) used parabolic dish concentrators to focus the sun-rays on the receiver for obtaining a high temperature of work fluid. Furthermore, they designed a cylindrical closed-tube open-cavity solar receiver in such a way to absorb the solar energy to the maximum extent [27]. Other methods have also been applied to achieve high concentration ratio. Liang et al. (2015) investigated solar concentrator based on the off-axis toroidal confocal relay principle which can be able to collect, converge, and re-collimate the solar beam and also owing the properties of higher concentration ratio and thin aspect ratio [28]. Dähler et al. (2016) used resilient inflatable plastic films as reflective materials in a dish concentrator [29]. Canavarro et al. (2016) developed a novel compound elliptical-type concentrator for a parabolic primary with a tubular receiver [30]. Tsai (2015 and 2016) adopted free-form surfaces as reflective surfaces [31,32].

In the solar PV system, Ricardo Perez-Enciso et al. (2016) designed a point focus solar concentrator composed of 18 spherical mirrors mounted on an equatorial solar tracker. Each mirror was 30 cm in diameter and 1.9 cm in thickness with the global reflecting area of 1.274 m^2. This solar concentrator was initially designed to obtain a spot of 2.5 cm in diameter [33]. Meng et al. (2016) proposed the concept of novel free-form Cassegrain concentrator (FFCC) formed by the classic dish concentrator and a secondary free-form reflector with the aim of achieving higher concentration for a thermal receiver [34]. Generally, Fresnel lens is the common element in order to achieve a high concentration ratio. A proposed photovoltaic system based on multiple Fresnel lens primaries achieved unreached concentration levels so far [35]. Similarly, solar CPV device using LFR concentrator had relatively higher solar concentrating uniformity than that of the parabolic trough concentrator at same geometric concentration ratio [36]. Zheng et al. (2014) devised a cylindrical compound Fresnel solar concentrator consisting of an arched Fresnel lens, a Fresnel mirror, and a secondary reflector and achieved up to 84% optical efficiency [37]. Sahin et al. (2019) proposed two-stage optical systems composed of a Fresnel lens with an aspherical surface as a primary element and a planar element with a diffractive surface as the second element. The combined system could achieve up to 0.87 optical efficiency [38]. Recently, multi-segment mirror hybrid solar concentration system has been developed using spectral beam splitting technology providing high uniformity of solar radiation flux density distribution on solar cells [6].

However, to date, nobody has employed multiple aspheric reflectors to achieve a higher concentration ratio for off-axis point focusing. Aspheric reflectors can remove the aberrations efficiently and it is anticipated that solar spot would decrease the diameter to achieve the high solar concentration ratio. Based on our previous work [14], we designed an off-axis point focused solar concentrator system consisting of 190 aspheric reflectors by employing particle swarm optimization

(PSO) method. PSO algorithm was successfully implemented for designing the laser beam shaping lenses and LED collimator systems [39–41] in our recent works.

2. Focusing Principles of a Single Aspheric Reflector

2.1. Ideas of Focusing

Figure 1 depicts a new idea about a concentrator system. This system has multiple reflectors which reflectively focus sunlight on the same small areas. If the number of such reflectors is large enough, the concentration ratio will also be high enough, and the focused spot can reach very high temperatures.

Reflecting surfaces employ even-aspheric surfaces whose expression is shown in Equation (1).

$$y = \frac{Ch^2}{1 + \sqrt{1 - h^2C^2(1 + a_2)}} + a_4h^4 + a_6h^6 + a_8h^8 \quad (1)$$

$h = \sqrt{x^2 + z^2}$ in Equation (1). The first term in the above equation corresponds to a quadric surface, C is the apex curvature of a quadric surface, $1 + a_2$ is the coefficient of a quadric surface, a_2 relates with the eccentricity of a quadric surface, a_4, a_6, a_8 are higher order polynomial coefficients of an aspheric equation, respectively.

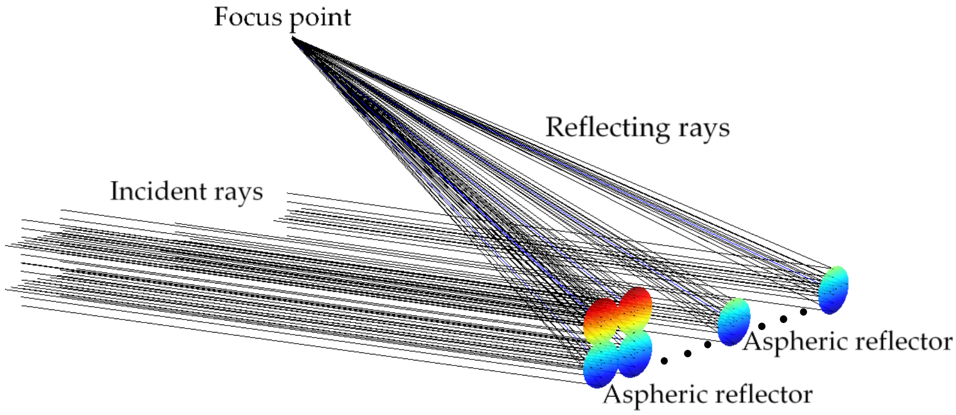

Figure 1. The focusing system consists of multiple aspheric reflectors.

If $a_4 = a_6 = a_8 = 0$, then Equation (1) is simplified to $y = \frac{Ch^2}{1+\sqrt{1-h^2C^2(1+a_2)}}$, this is a rotational quadric surface around the symmetry Y-axis. Equation (1) respectively defines a hyperboloid, paraboloid, ellipsoid, and spherical with different a_2 values.

2.2. Analysis for Focusing Action of a Single Aspheric Reflector

A Cartesian coordinate system is established as shown in Figure 2; the coordinate origin O is located at the apex of an aspheric reflector. In Figure 2, we draw three incident-reflecting rays passing through the reflector, one of them travels through the vertex O of the aspheric surface, and the other two do not travel through O. Let the angle between an incident ray passing through the vertex O and the surface normal at O be θ (incident angle), then the angle of reflection must also be θ. As long as this incident ray is given, the reflected ray is also determined, which has nothing to do with the shape of the aspheric surface. Therefore, the focal point must be placed on the reflected light ray passing through the apex point O. Let the incident solar beam be parallel to the xoy plane, then the Z coordinate of any point on the reflected light ray through O must be zero. Take any point Pf $(x', y', 0)$ on this ray as the center of a focal spot, accordingly, the relationship between x' and y' is $x' = -y'\tan\theta$.

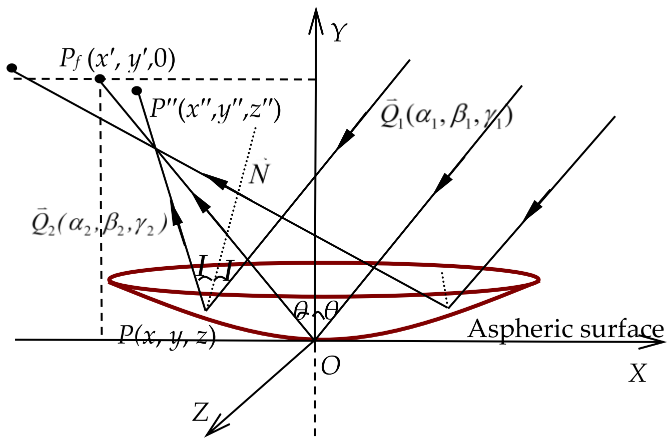

Figure 2. The relative position relation among incident rays, reflected rays and the focus point.

The reflected light vector $\overrightarrow{Q_2}(\alpha_2, \beta_2, \gamma_2)$ is approximately obtained by the following method described in brief [14]. Given that the unit vector $\overrightarrow{Q_1}(\alpha_1, \beta_1, \gamma_1)$ of incidence ray, a point on an incident ray and an aspheric equation, a ray intersection point P (x, y, z) at the aspheric reflecting surface can be gotten using approximate methods, thus the normal vector $\overrightarrow{N}(\alpha_N, \beta_N, \gamma_N)$ at the intersection point can be determined by the aspheric equation. According to the vector law of reflection, the unit direction vector $\overrightarrow{Q_2}(\alpha_2, \beta_2, \gamma_2)$ of reflected ray can be found from $\overrightarrow{Q_1}$ and $\overrightarrow{N}$.

$$\overrightarrow{Q_2} = \overrightarrow{Q_1} + g\overrightarrow{N} \tag{2}$$

where, $g = -2\left|\alpha_1\alpha_N + \beta_1\beta_N + \gamma_1\gamma_N\right|$.

We can see from the above expression that $\overrightarrow{Q_2}$ is only a function of $\overrightarrow{Q_1}$ and $\overrightarrow{N}$, $\overrightarrow{N}$ is only a function of aspheric parameters C, a_2, a_4, a_6, a_8 and intersection point P, and intersection point P is determined by $\overrightarrow{Q_1}$ and the aspheric parameters. When $\overrightarrow{Q_1}$ is given, intersection point P is just determined by the aspheric parameters, therefore, $\overrightarrow{N}$ is also obtained only from aspheric parameters. In this case, given $\overrightarrow{Q_1}$, $\overrightarrow{Q_2}$ is just a function of the aspheric parameters C, a_2, a_4, a_6, a_8. As long as these parameters are properly selected, we can find a suitable $\overrightarrow{Q_2}$ directing the neighborhood of the focal point, thereby the objective of focusing the sunbeams on a small area can be achieved. Since it has been assumed that the incident solar beam is parallel to the xoy plane, thus $\gamma_1 = 0$ in $\overrightarrow{Q_1}(\alpha_1, \beta_1, \gamma_1)$.

2.3. Analyses for Collecting Solar Light with a Single Reflector

As shown in Figure 2, take a point $P_f\,(x', y', 0)$ on a reflected light ray passing through the vertex O as a focus point. $P''\,(x'', y'', z'')$ is a point on a reflected light ray not passing through O, it is known from Figure 2 that a relation of x'', z'', and y'' is determined by the following formula:

$$\begin{cases} x'' = x + \frac{\alpha_2}{\beta_2}(y'' - y) \\ z'' = z + \frac{\gamma_2}{\beta_2}(y'' - y) \end{cases} \tag{3}$$

where, x, y, and z are coordinates of intersection P between the light ray and the aspheric reflector. Let y'' = y', then the distance between point P'' and the focus point P' is given by $R = \sqrt{(x'' - x')^2 + (z'' - 0)^2}$, the smaller the R value, the better the focusing effect. It can be seen from the above analysis that R is also only a function of aspheric parameters. The appropriate R-value can be gotten as long as we properly select these parameters. In this paper, let R be less than a certain value, this certain value is used as the maximum allowable value of the fitness function of the PSO algorithm, and aspheric parameters

C, a_2, a_4, a_6, a_8 can be found by PSO techniques. Here we would like to point out that in order to better understand our specific implementation of the algorithm, readers should have knowledge about PSO.

For example, let the incident angle θ = 25°, and the focus point be P' (400*tan25°, 400, 0), then $R = \sqrt{(x'' + 186.5231)^2 + z''^2}$. Evenly taking multiple incident rays on a reflecting surface, their corresponding reflected rays have the respective R-values, and all R-values are summed up, then we have:

$$\sum_i R_i = \sum_i \sqrt{(x_i'' + 186.5231)^2 + z_i''^2}$$

Here, i denotes the ith light ray. $\sum\limits_i R_i$ serves as the fitness function of PSO, aspheric parameters C, a_2, a_4, a_6, a_8 can be obtained by seeking the particle with the smallest $\sum\limits_i R_i$ using the PSO method [41].

3. The Construction of a New Coordinate System When Vertices of Aspheric Reflectors Do Not Locate at the Origin of the Coordinate System

3.1. The Construction of a New Coordinate System and Coordinate Transformations between the Old and the New Coordinate System

As shown in Figure 3, the vertex of another reflector of a solar concentrator system is not at the origin O of the coordinate system, but at point O' (a, b, c). The point P_f $(-y_f \tan\theta, y_f, 0)$ is still the focus point, then a vector along the direction of $O'P_f$ is $\overrightarrow{O'P_f} = (-y_f \tan\theta - a, y_f - b, -c)$, $\vec{Q}_1(\alpha_1, \beta_1, \gamma_1)$ is a unit vector along incident rays in the xyz coordinate system, $\alpha_1 = -\sin\theta$, $\beta_1 = -\cos\theta$, $\gamma_1 = 0$. The angle $2\theta_1$ between $\overrightarrow{O'P_f}$ and $-\vec{Q}_1$ is:

$$\cos(2\theta_1) = \frac{(y_f \tan\theta + a)\alpha_1 - (y_f - b)\beta_1}{\sqrt{(y_f \tan\theta + a)^2 + (y_f - b)^2 + c^2}} \tag{4}$$

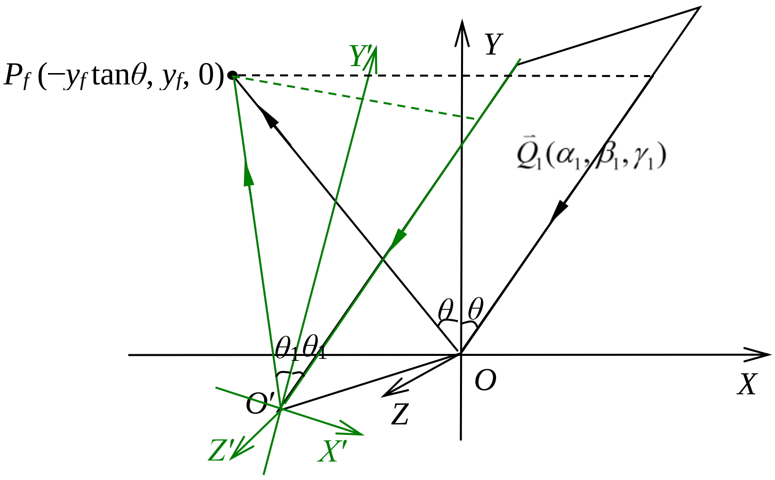

Figure 3. The schematic diagram of incident ray and reflecting ray at the vertex of curved surface.

The vector along the bisector of the angle is:

$$\frac{1}{\left|\overrightarrow{O'P_f}\right|}\overrightarrow{O'P_f} - \vec{Q}_1 = \Big(\frac{-y_f \tan\theta - a}{\sqrt{(y_f \tan\theta + a)^2 + (y_f - b)^2 + c^2}} - \alpha_1, \frac{y_f - b}{\sqrt{(y_f \tan\theta + a)^2 + (y_f - b)^2 + c^2}} - \beta_1, \frac{-c}{\sqrt{(y_f \tan\theta + a)^2 + (y_f - b)^2 + c^2}}\Big) \tag{5}$$

Let $A_1 = \frac{-y_f \tan\theta - a}{\sqrt{(y_f \tan\theta + a)^2 + (y_f - b)^2 + c^2}} - \alpha_1$, $A_2 = \frac{y_f - b}{\sqrt{(y_f \tan\theta + a)^2 + y'^2 + c^2}} - \beta_1$ $A_3 = \frac{-c}{\sqrt{(y_f \tan\theta + a)^2 + (y_f - b)^2 + c^2}}$.

The direction cosines of the vector of angle bisector are:

$$\cos\alpha_2' = \frac{A_1}{\sqrt{{A_1}^2 + A_2^2 + A_3^2}}, \cos\beta_2' = \frac{A_2}{\sqrt{{A_1}^2 + A_2^2 + A_3^2}}, \cos\gamma_2' = \frac{A_3}{\sqrt{{A_1}^2 + A_2^2 + A_3^2}} \tag{6}$$

Let the normal vector to the plane constituted by the vector $\vec{Q}_1$ and the vector $\overrightarrow{O'P_f}$ be $\overrightarrow{O'Z'}$

$$\begin{aligned} \overrightarrow{O'Z'} &= -\vec{Q}_1 \times \overrightarrow{O'P_f} = -\begin{vmatrix} \vec{i} & \vec{j} & \vec{k} \\ \alpha_1 & \beta_1 & 0 \\ -y_f \tan\theta - a & y_f - b & -c \end{vmatrix} \\ = -\begin{vmatrix} \beta_1 & 0 \\ y_f - b & -c \end{vmatrix} \vec{i} &+ \begin{vmatrix} \alpha_1 & 0 \\ -y_f \tan\theta - a & -c \end{vmatrix} \vec{j} - \begin{vmatrix} \alpha_1 & \beta_1 \\ -y_f \tan\theta - a & y_f - b \end{vmatrix} \vec{k} \\ &= \beta_1 c\,\vec{i} - \alpha_1 c\,\vec{j} - [\alpha_1(y_f - b) + \beta_1(y_f \tan\theta + a)]\,\vec{k} \end{aligned} \tag{7}$$

The direction cosines of $\overrightarrow{O'Z'}$:

$$\begin{aligned} \cos\alpha_3' &= \frac{\beta_1 c}{\sqrt{(\beta_1 c)^2 + (\alpha_1 c)^2 + [\alpha_1(y_f - b) + \beta_1(y_f \tan\theta + a)]^2}} \\ \cos\beta_3' &= -\frac{\alpha_1 c}{\sqrt{(\beta_1 c)^2 + (\alpha_1 c)^2 + [\alpha_1(y_f - b) + \beta_1(y_f \tan\theta + a)]^2}} \end{aligned} \tag{8}$$

$$\cos\gamma_3' = -\frac{\alpha_1(y_f - b) + \beta_1(y_f \tan\theta + a)}{\sqrt{(\beta_1 c)^2 + (\alpha_1 c)^2 + [\alpha_1(y_f - b) + \beta_1(y_f \tan\theta + a)]^2}}$$

Take the vector along the angle bisector as the positive direction of the Y' axis of a new coordinate system, and $\overrightarrow{O'Z'}$ as the positive direction of the Z' axis of a new coordinate system, then the positive direction of the X' axis is also determined. In the XYZ coordinate system, direction cosines of the X' axis are:

$$\overrightarrow{O'X'} = \overrightarrow{O'Y'} \times \overrightarrow{O'Z'} = \begin{vmatrix} \vec{i} & \vec{j} & \vec{k} \\ \cos\alpha_2' & \cos\beta_2' & \cos\gamma_2' \\ \cos\alpha_3' & \cos\beta_3' & \cos\gamma_3' \end{vmatrix} = \tag{9}$$

$$\begin{vmatrix} \cos\beta_2' & \cos\gamma_2' \\ \cos\beta_3' & \cos\gamma_3' \end{vmatrix} \vec{i} - \begin{vmatrix} \cos\alpha_2' & \cos\gamma_2' \\ \cos\alpha_3' & \cos\gamma_3' \end{vmatrix} \vec{j} + \begin{vmatrix} \cos\alpha_2' & \cos\beta_2' \\ \cos\alpha_3' & \cos\beta_3' \end{vmatrix} \vec{k}$$

Let: $\cos\alpha_1' = \begin{vmatrix} \cos\beta_2' & \cos\gamma_2' \\ \cos\beta_3' & \cos\gamma_3' \end{vmatrix}, \cos\beta_1' = -\begin{vmatrix} \cos\alpha_2' & \cos\gamma_2' \\ \cos\alpha_3' & \cos\gamma_3' \end{vmatrix}, \cos\gamma_1' = \begin{vmatrix} \cos\alpha_2' & \cos\beta_2' \\ \cos\alpha_3' & \cos\beta_3' \end{vmatrix}$.

Then:

$$\overrightarrow{O'X'} = \cos\alpha_1' \vec{i} + \cos\beta' \vec{j}_2 + \cos\gamma_1' \vec{k} \tag{10}$$

The coordinate transformation between the two coordinate systems satisfies the following transforming relationships:

$$y = \begin{cases} x = x' \cos\alpha 1' + y' \cos\alpha 2' + z' \cos\alpha 3' + a \\ y = x' \cos\beta 1' + y' \cos\beta 2' + z' \cos\beta 3' + b \\ z = x' \cos\gamma 1' + y' \cos\gamma 2' + z' \cos\gamma 3' + c \end{cases} \tag{11}$$

Writing the above equations in matrix form we get:

$$\begin{pmatrix} x \\ y \\ z \end{pmatrix} = \begin{pmatrix} \cos\alpha'_1 & \cos\alpha'_2 & \cos\alpha'_3 \\ \cos\beta'_1 & \cos\beta'_2 & \cos\beta'_3 \\ \cos\gamma'_1 & \cos\gamma'_2 & \cos\gamma'_3 \end{pmatrix} \begin{pmatrix} x' \\ y' \\ z' \end{pmatrix} + \begin{pmatrix} a \\ b \\ c \end{pmatrix} \tag{12}$$

3.2. Parameter Optimization of Aspheric Surfaces Whose Vertices Locate at the Origin of the New Coordinate System

As shown in Figure 4, the vertex of an aspheric reflector locates at the origin O' of the new coordinate system. The incident angle θ_1 of light ray passing through the origin O' can be calculated with Equation (4). In the new coordinate system, unit vectors $\vec{Q}_1(\alpha_1, \beta_1, \gamma_1)$ along the incident light rays can be gotten from θ_1, $\alpha_1 = -\sin\theta_1$, $\beta_1 = -\cos\theta_1$, $\gamma_1 = 0$. Focus point coordinates in the new coordinate system can be solved using Equations (11) or (12). Therefore, in the X′Y′Z′ coordinate system, given $\vec{Q}_1$ and focus point coordinates, according to the analysis in Sections 2.2 and 2.3, just like in the XYZ coordinate system, we can also find aspheric parameters C, a_2, a_4, a_6, a_8 with the smallest fitness value in the $X'Y'Z'$ reference system. In this way, we will obtain aspheric parameters of another series of optimal aspheric reflectors constituting a concentrator system.

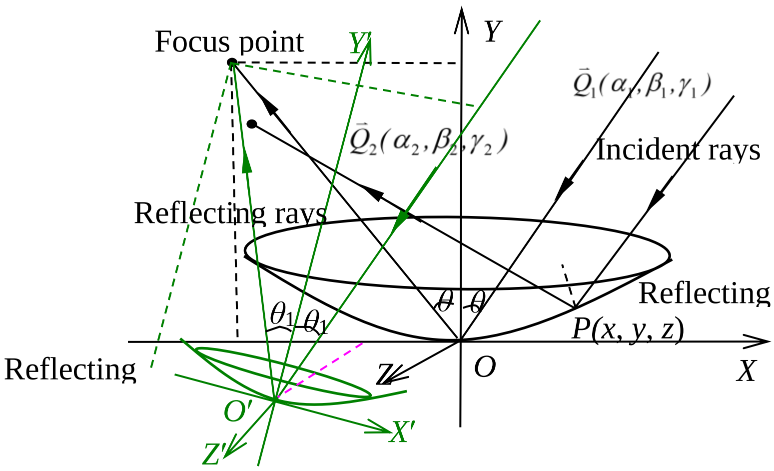

Figure 4. The aspheric reflector whose vertex is not at point *O*.

4. Examples of Seeking Optimal Aspheric Parameters

4.1. Seeking Parameters of the Optimal Aspheric Surface Whose Vertex Is the XYZ Coordinate Origin

As shown in Figure 4, let $\theta = 25°$, and the coordinates of focus point in XYZ space be P_f (−186.5231, 400, 0). In the XOZ plane, we uniformly pick multiple incident points on the circle with center O and radius 10 cm, as shown in Figure 5a,b. Figure 5b shows that a square with a side length of 20 cm is divided into 2N × 2N uniform grids, and these grid nodes are used as incident points at which light rays (or their virtual extension) strike the XZ plane. These nodes will be reserved while their distance from the origin O is less than 10 cm, otherwise, they will be deleted. Thus, multiple incident light rays evenly hitting the aspheric reflector will be gotten. Taking $N = 5$, $\sum_i R_i = \sum_i \sqrt{(x''_i + 186.5231)^2 + {z''_i}^2}$ of all the reflected light rays can be obtained from Equation (3). $\sum_i R_i$ is used as the fitness function of the PSO algorithm. In this design example, the number of parameter variables C, a_2, a_4, a_6, a_8 controlling the shape of a reflector is the dimension of each particle's position vector, the searching range of each variable is based on a sensitivity analysis of effects of function parameters, and respectively set as $C[-1/1500, 0]$, $a_2[0, 200]$, $a_4[-5 \times 10^{-8}, 5 \times 10^{-8}]$, $a_6[-10^{-11}, 10^{-11}]$, $a_8[-10^{-13}, 10^{-13}]$. The smallest

$\sum_i R_i$ is searched for by the standard PSO tool written in matlab, and then a definite set of aspheric parameters with the smallest $\sum_i R_i$ will be attained [41]. Here we once again emphasize that readers should have basic knowledge about PSO.

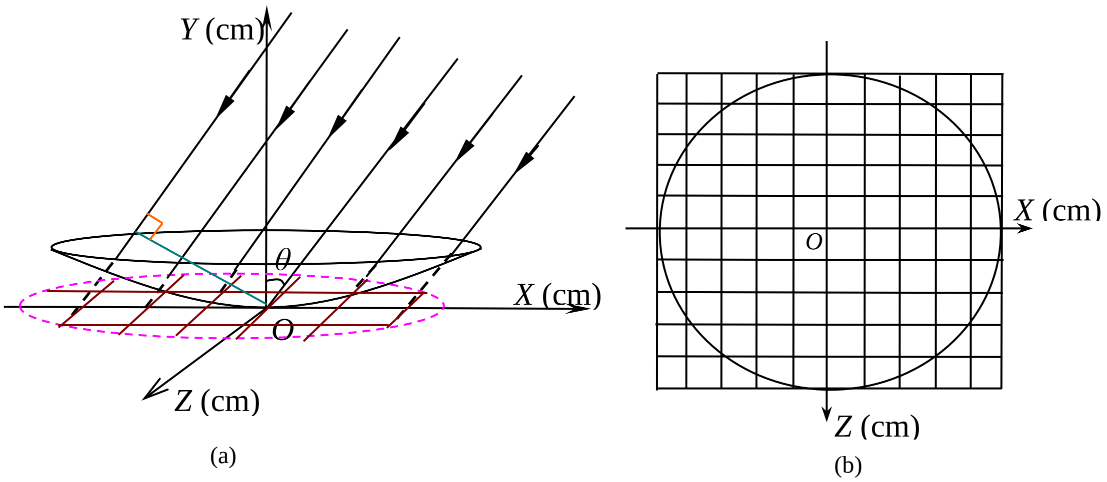

Figure 5. The diagrammatic sketch of the aperture of incident solar beam. (**a**) side view of the incident ray with a radius of 10 cm; (**b**) top view of the incident ray with a side length of 20 cm.

4.2. Seeking Parameters of the Optimal Aspheric Surface Whose Vertex Is at the Origin of the $X'Y'Z'$ Coordinate System

For the O'- $X'Y'Z'$ coordinate system, coordinates of point O' in the XYZ coordinate system are (a, b, c), and the positive direction cosines of X', Y', and Z'-axis in the XYZ coordinate system can be calculated with Equations (6), (8), and (9), respectively. The coordinates of focus point P_f in the $X'Y'Z'$ coordinate system can be worked out through Equation (10), and the angle θ_1 between an incident light ray and Y' -axis can be calculated using Equation (4). An incident ray vector $\overrightarrow{Q_1}(\alpha_1, \beta_1, \gamma_1)$ in the $X'Y'Z'$ coordinate system is obtained from θ_1, $\alpha_1 = -\sin\theta_1$, $\beta_1 = -\cos\theta_1$, $\gamma_1 = 0$. We can also use the PSO algorithm to seek aspheric parameters to suit our needs in the $X'Y'Z'$ coordinate system, just as in the XYZ coordinate system.

For example, the coordinates of point O' in the XYZ coordinate system are (−100, 0, 40), namely $a = -100$, $b = 0$, $c = 40$, then we establish the $X'Y'Z'$ coordinate system according to Equations (6), (8), and (9). Thus, we can calculate from Equation (10) that P_f (−186.5231, 400, 0) in the XYZ coordinate system is transformed into $P_f{}'$(−132.3867, 389.3071, 0) in the $X'Y'Z'$ coordinate system. From Equation (4), we have $\theta_1 = 18.7810°$. Therefore, in the $X'Y'Z'$ coordinate system, $\overrightarrow{Q_1}(\alpha_1, \beta_1, \gamma_1)$ is gotten from $\alpha_1 = -\sin 18.7810°$, $\beta_1 = -\cos 18.7810°$, $\gamma_1 = 0$. The known $\overrightarrow{Q_1}$ and $P_f{}'$, we can use the same method as in the XYZ coordinate system to find the aspheric parameters in the $X'Y'Z'$ coordinate system: $C = -1/828.2705$, $a_2 = 34.6162$, $a_4 = -2.7765 \times 10^{-9}$, $a_6 = -1.8671 \times 10^{-11}$, $a_8 = -5.0820 \times 10^{-15}$. The focused spot radius max (R_i) = 0.5580 cm. Figure 6 shows the focused results of an designed aspheric reflector. We can imagine from this figure that if there are many such aspheric reflectors whose vertex locates at different locations, and each aspheric reflector focuses the sunlight beam into the same small area, then the purpose of improving the concentration ratio will be achieved.

Figure 7 shows the relative position of each aspheric reflector vertex in a concentrator system. First, all reflector vertices are located in the XOZ plane. Second, they all are at the grid nodes as shown in Figure 7. Watching along the Z direction, all reflectors are placed in 10 rows, each row has 21 reflectors from first to eighth row, the ninth row has 15 reflectors, and the tenth row has 7 reflectors; thus this concentrating system consists of a total of 190 reflectors. The distance between two vertices of adjacent aspheric reflectors in the same row is 20 cm.

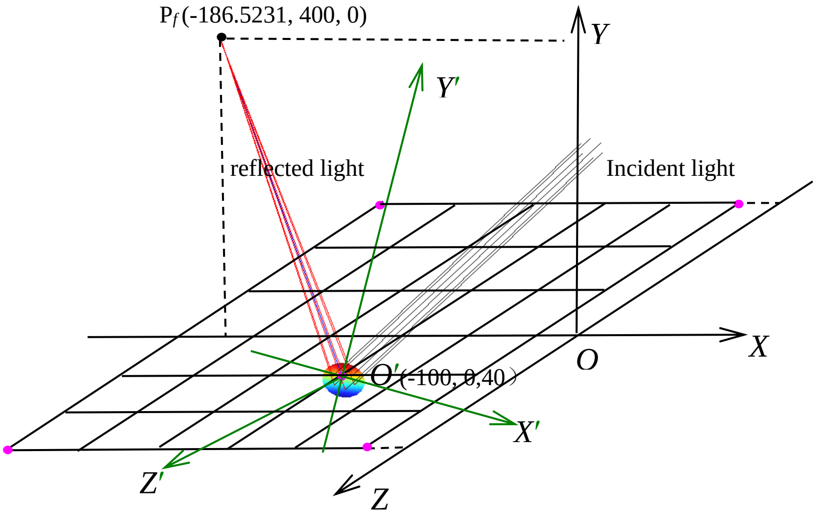

Figure 6. The focused result of a designed aspheric reflector whose vertex is not origin O of the XYZ system (in units of cm).

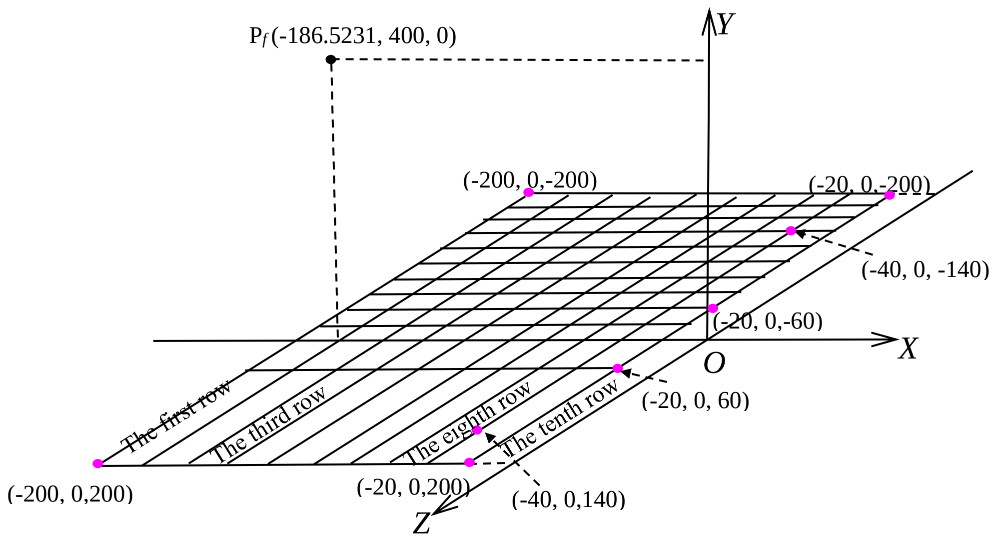

Figure 7. The schematic diagram for vertex positions of aspheric reflectors in the coordinate system (in units of cm).

One by one, we use the above method to find aspheric parameters C, a_2, a_4, a_6, a_8 of each reflector. Table 1 lists the optimization results of aspheric parameters of 21 reflectors in the eighth row, and the last column of Table 1 is the maximum spot radius being brought about by each aspheric reflector. Because of the limitation of length, the optimization results for 169 other groups of aspheric parameters are not listed.

This concentrator system has a total of 190 aspheric reflectors, the sunlight receiving area of each reflector in the plane vertical to the light beam is $\pi[10\cos\ (25^0)]^2$ cm^2 as shown in Figure 5a, the focused spot radius is no more than 1 cm. So the concentration ratio of the entire concentrator systems is calculated to be 15606:1. Of course, the number of aspheric reflectors is still appropriately added to thereby increase the concentration ratio of the concentrator systems.

In the above analysis, we take the sun as the point sun. In fact, solar rays are not strictly parallel to each other, but with a 2σ included angle as shown in Figure 8, and σ = 16′. In the XY plane, the theoretical diameter of the sun's image formed by reflection of light from any point on the reflector is calculated by the following equation, $D = \frac{d}{\cos\theta} = \frac{2R\tan 16'}{\cos\theta}$, here R is the distance between point P and the intersection P_f of a reflected ray and the focal plane, and its value changes slightly with the change of reflection point P. R can be obtained by using the two-point distance formula, and the incident angle θ can be calculated from vectors α_2 and β_2 of a reflected ray at point P, $\cos\theta = \left|\frac{\alpha_2}{\sqrt{\alpha_2^2+\beta_2^2}}\right|$. In the present embodiment, R ≈ 4.5 m, $\theta \approx 24°$, then D ≈ 4.6 cm, therefore, there is 4.6 times the error between the actual spot and the spot obtained by using the point sun. Hence, the corrected concentration ratio is 3393.

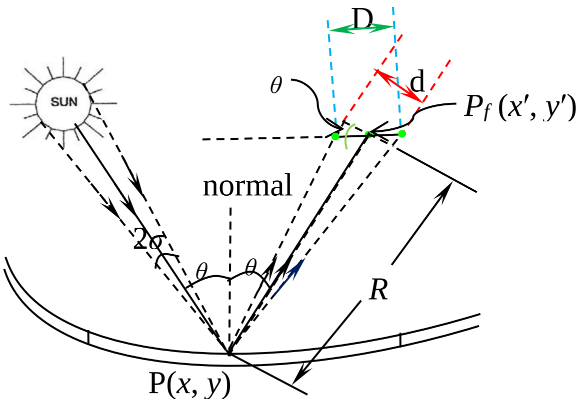

Figure 8. While the solar beam is actually a cone beam with a solid angle of 32′, the focus spot will be extended.

Table 1. The parameters of aspheric reflectors whose vertices are located at different positions obtained with the particle swarm optimization algorithm.

Aspheric Vertex Coordinates (cm)	$r = 1/C$ (cm)	a_2	a_4	a_6	a_8	Max (R_i)
(−60, 0,200)	−960.0	112.3796	-3.8535×10^{-8}	5.0000×10^{-11}	-1.2403×10^{-14}	1.0000
(−60, 0,180)	−932.9969	88.3578	-1.0400×10^{-8}	3.7394×10^{-11}	-5.0000×10^{-14}	0.9735
(−60, 0,160)	−915.8788	33.9926	-1.8546×10^{-8}	3.7024×10^{-11}	-2.2159×10^{-14}	0.9285
(−60, 0,140)	−900.6793	24.1044	-7.0350×10^{-9}	-5.0000×10^{-11}	-5.0000×10^{-14}	0.8844
(−60, 0,120)	−887.8191	45.6911	-4.0313×10^{-10}	-5.0000×10^{-11}	-3.0517×10^{-14}	0.8611
(−60, 0,100)	−876.9833	52.5050	-1.6645×10^{-8}	5.0000×10^{-11}	-5.0000×10^{-14}	0.8238
(−60, 0,80)	−866.0193	50.0	3.8941×10^{-9}	-5.0000×10^{-11}	-5.0000×10^{-15}	0.7979
(−60, 0,60)	−861.4021	21.1483	-2.8481×10^{-8}	4.7987×10^{-11}	2.8180×10^{-14}	0.7717
(−60, 0,40)	−860.0	60.0000	-2.7203×10^{-8}	-3.6588×10^{-12}	-8.0359×10^{-15}	0.7508
(−60, 0,20)	−851.1841	50.0000	-5.5993×10^{-9}	-1.3237×10^{-12}	3.3003×10^{-14}	0.7577
(−60, 0,0)	−850.1531	39.1247	-4.6066×10^{-9}	-2.4065×10^{-11}	-1.7072×10^{-15}	0.7520
(−60, 0, −20)	−860.0	108.9231	-4.0558×10^{-8}	4.8699×10^{-11}	4.5294×10^{-14}	0.7309
(−60, 0, −40)	−856.2597	53.8495	-1.7924×10^{-8}	1.6465×10^{-11}	3.3017×10^{-14}	0.7555
(−60, 0, −60)	−860.6008	138.2402	7.7073×10^{-9}	-2.0915×10^{-12}	-4.4140×10^{-15}	0.7779
(−60, 0, −80)	−868.1085	0.8521	-1.8913×10^{-8}	-2.0171×10^{-11}	-1.3113×10^{-14}	0.7943
(−60, 0, −100)	−876.6630	3.9000	-1.9007×10^{-8}	1.6750×10^{-11}	-3.8802×10^{-14}	0.8267
(−60, 0, −120)	−888.1854	37.8347	-1.3108×10^{-8}	2.0836×10^{-12}	-1.4232×10^{-15}	0.8555
(−60, 0, −140)	−890.3378	−94.1528	1.6813×10^{-8}	5.6164×10^{-12}	-5.0000×10^{-14}	0.9515
(−60, 0, −160)	−915.5987	−18.1712	-2.0586×10^{-8}	-2.6041×10^{-12}	1.3613×10^{-14}	0.9298
(−60, 0, −180)	−933.2251	−39.6372	-2.2386×10^{-8}	-2.6279×10^{-11}	2.5424×10^{-14}	0.9749
(−60, 0, −200)	−951.6965	−14.6271	-1.4399×10^{-8}	-5.0000×10^{-11}	-2.2127×10^{-14}	1.0000

4.3. Computer Simulations of Focusing Effect

Figure 9a is the focusing simulation of three aspheric reflectors, and the three local coordinate systems for three reflectors and the global coordinate system *XYZ* are also shown in the figure. In the simulation process, we first calculate the coordinate values of each desired point in the local coordinate system, and then convert these local coordinate values to the global coordinate system using Equations (11) or (12).

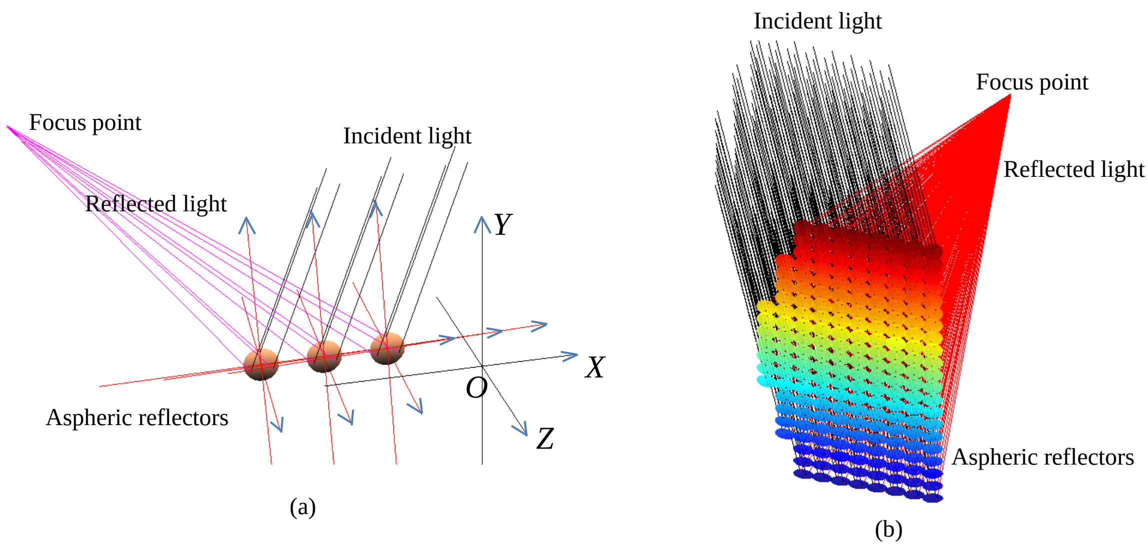

Figure 9. The optical path simulation of the concentrator system. (**a**) The optical path diagram of three aspheric reflectors; (**b**) the optical path diagram of 190 aspheric reflectors.

Figure 9b shows the optical path simulation of the concentrator system consisting of 190 aspheric reflectors. It is shown that sunlight beams irradiating on 190 aspheric reflectors are reflected and focused in the same small area, so the idea of focusing sun beams in Section 2 of this paper can be realized.

It can also be seen from Figure 9a,b that such a concentrator system can have better off-axis focus than a rotation paraboloid. If the light receiving aperture of each reflector is reduced, then in the meantime the number of reflectors is increased; the smaller focused spot will be gotten. If necessary, the smaller focused spot can be turned into a parallel beam with a powerful energy, so that it can be further exploited.

4.4. Verifying the Correctness of Designed Datum with Zemax Software

The datum in the first row of Table 1 is selected. It can be known from this row that the vertex coordinate of the reflector in the old coordinate system (global coordinate system) is (−60, 0, 200), establishing a new coordinate system (local coordinate system) whose origin is the vertex of the reflector. In this local coordinate system, the coordinate of focus point is obtained from Equation (10) and is (−190.2248, 424.0550, 0). Designed aspheric parameters are $C = -1/960.0$, $a_2 = 112.3796$, $a_4 = -3.8535 \times 10^{-8}$, $a_6 = 5.00 \times 10^{-11}$, $a_8 = -1.2403 \times 10^{-14}$, respectively. The angle θ_1 between the incident solar rays and Y′ axis of the local coordinate system can be calculated from Equation (4) and is 24.1603°. Let the beam diameter be 10 cm. The aspheric parameters, the viewing angle θ_1, and the aperture value (beam diameter) are inputted to Zemax software as shown in Figure 10a, and the optical path through the reflector is also shown in Figure 10a. Figure 10b is the optical path simulated with a self-compiled Matlab program. By comparing Figure 10a,b, the spot radius obtained in Matlab and Zemax are about 1 mm and 990 µm, respectively, which means that both design results and self-compiled programs are correct. In this way, we can verify the correctness of the design of each reflector, and the correctness of the whole system design is also verified.

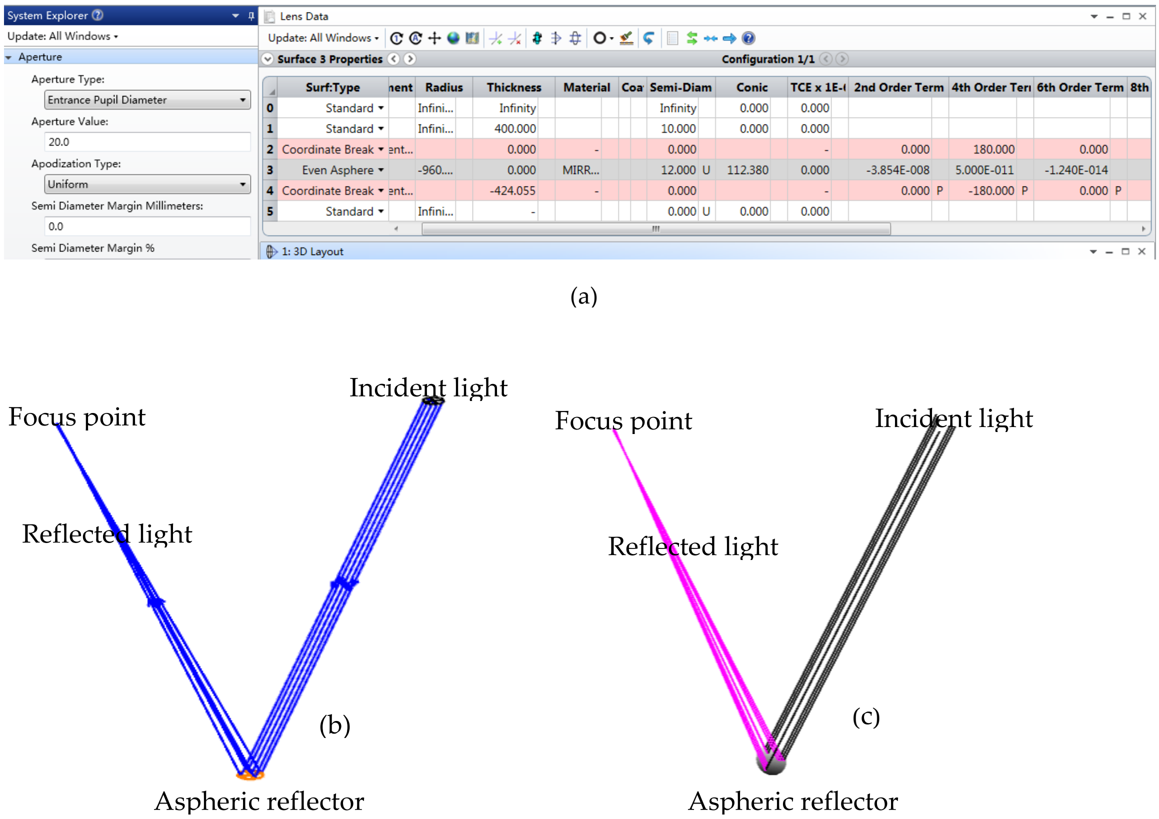

Figure 10. The light paths simulated with Zemax and self-compiled programs. (**a**) The input parameters in the Lens Data Editor of Zemax; (**b**) the ray tracing using the Zemax software; (**c**) the ray tracing using a self-compiled Matlab program.

5. Conclusions

In this study, we chose 25° special incident angle (between the incident ray and Y-axis) and designed an off-axis focused solar concentrator system consisting of 190 aspheric reflectors with 10 cm in radius and 3 mm in thickness. These aspheric reflectors were arranged in 10 rows. The detailed arrangement is listed as follows: row 1 to 8 contained 21 reflectors, row 9 contained 15 reflectors, and row 10 contained 7 reflectors. The vertex of each reflector lied in the same plane and located in the area defined by the four coordinates (−200, 0, 200), (−20, 0, 200), (−20, 0, −200), and (−200, 0, −200). The distance between two vertices of adjacent aspheric reflectors was 20 cm and the focusing point of each reflector was located on coordinate (−186.5231, 400, 0). The system had theoretical concentration ratio of 3393:1 and the focused spot radius was less than 1 cm. This type of concentrating solar power system can be used in the solar thermal utilization under high temperature, concentrating solar power (CSP) plants, and solar-pumped lasers. This system has an important scientific significance for the development of solar energy utilization technology and has an important practical significance for environmental protection. In our future work, we will further optimize our current systems with reflectors of different designs, parameters, and even different optimization algorithms [42–44].

Author Contributions: Data curation, G.C. and H.Q.; Investigation, H.Q.; Project administration, H.Q. and B.L.; Supervision, B.L.; Writing—review and editing, R.R.

Funding: This research was funded by Shandong Provincial Natural Science Foundation (ZR2019MA071) and APC was funded by Beijing Railway Century Soil Engineering Co., LTD, Yangfangdian Road, Haidian District, Beijing 100038, China.

Acknowledgments: The authors would like to thank the financial support from Shandong Provincial Natural Science Foundation (ZR2019MA071).

Conflicts of Interest: The authors declare no conflict of interest.

References

1. Shah, T.R.; Ali, H.M. Applications of hybrid nanofluids in solar energy, practical limitations and challenges: A critical review. *Sol. Energy* **2019**, *183*, 173–203. [CrossRef]
2. Ahmadi, M.H.; Ghazvini, M.; Sadeghzadeh, M.; Nazari, M.A.; Ghalandari, M. Utilization of hybrid nanofluids in solar energy applications: A review. *Nano-Struct. Nano-Objects* **2019**, *20*, 100386. [CrossRef]
3. Abid, M.; Ratlamwala, T.H.A.; Atikol, U. performance assessment of parabolic dish and parabolic trough solar thermal power plant using nanofluids and molten salts. *Int. J. Energy Res.* **2016**, *40*, 550–563. [CrossRef]
4. Singh, G. Solar power generation by PV (photovoltaic) technology: A review. *Energy* **2013**, *53*, 1–13. [CrossRef]
5. Siddiqui, R.; Kumar, R.; Jha, G.K.; Gowri, G.; Morampudi, M.; Rajput, P.; Lata, S.; Agariya, S.; Dubey, B.; Nanda, G.; et al. Comparison of different technologies for solar PV (Photovoltaic) outdoor performance using indoor accelerated aging tests for long term reliability. *Energy* **2016**, *107*, 550–561. [CrossRef]
6. Wang, G.; Yao, Y.; Chen, Z.; Hu, P. Thermodynamic and optical analyses of a hybrid solar CPV/T system with high solar concentrating uniformity based on spectral beam splitting technology. *Energy* **2019**, *166*, 256–266. [CrossRef]
7. Daabo, A.M.; Mahmoud, S.; Al-Dadah, R.K. The effect of receiver geometry on the optical performance of a small-scale solar cavity receiver for parabolic dish applications. *Energy* **2016**, *114*, 513–525. [CrossRef]
8. Reddy, K.; Veershetty, G.; Vikram, T.S. Effect of wind speed and direction on convective heat losses from solar parabolic dish modified cavity receiver. *Sol. Energy* **2016**, *131*, 183–198. [CrossRef]
9. Yeh, N. Illumination uniformity issue explored via two-stage solar concentrator system based on Fresnel lens and compound flat concentrator. *Energy* **2016**, *95*, 542–549. [CrossRef]
10. Fernández, E.F.; Talavera, D.; Almonacid, F.M.; Smestad, G.P. Investigating the impact of weather variables on the energy yield and cost of energy of grid-connected solar concentrator systems. *Energy* **2016**, *106*, 790–801. [CrossRef]
11. Rovira, A.; Barbero, R.; Montes, M.J.; Abbas, R.; Varela, F. Analysis and comparison of Integrated Solar Combined Cycles using parabolic troughs and linear Fresnel reflectors as concentrating systems. *Appl. Energy* **2016**, *162*, 990–1000. [CrossRef]
12. Ng, K.M.; Adam, N.M.; Azmi, B.Z.; Wahab, M.A.; Sulaiman, M.Y. Field study of solar bowl under Malaysian tropical climate. *WSEAS Trans. Environ. Dev.* **2012**, *8*, 48–59.
13. Stine, W.B. *Power from the Sun: Principles of High Temperature Solar Thermal Technology*; Solar Energy Research Institute: Golden, CO, USA, 1987.
14. Qin, H.; Lei, C.; Liu, H.; Wang, Y.; Yuan, W. Optical design of an aspherical cylinder-type reflecting solar concentrator. *Energy* **2013**, *57*, 751–758. [CrossRef]
15. Li, Q.; Shirazi, A.; Zheng, C.; Rosengarten, G.; Scott, J.A.; Taylor, R.A. Energy concentration limits in solar thermal heating applications. *Energy* **2016**, *96*, 253–267. [CrossRef]
16. Burgess, G.; Lovegrove, K.; Mackie, S.; Zapata, J.; Pye, J. Direct steam generation using the SG4 500 m^2 paraboloidal dish concentrator. In Proceedings of the 17th SolarPACES Conference, Granada, Spain, 20–23 September 2011.
17. Rodriguez-Sanchez, D.; Rosengarten, G. Improving the concentration ratio of parabolic troughs using a second-stage flat mirror. *Appl. Energy* **2015**, *159*, 620–632. [CrossRef]
18. Balaji, S.; Reddy, K.S.; Sundararajan, T. Optical modeling and performance analysis of a solar LFR receiver system with parabolic and involute secondary reflectors. *Appl. Energy* **2016**, *179*, 1138–1151. [CrossRef]
19. Benyakhlef, S.; Al Mers, A.; Merroun, O.; Bouatem, A.; Boutammachte, N.; El Alj, S.; Ajdad, H.; Erregueragui, Z.; Zemmouri, E.; Ossama, M. Impact of heliostat curvature on optical performance of Linear Fresnel solar concentrators. *Renew. Energy* **2016**, *89*, 463–474. [CrossRef]
20. Sharma, V.; Nayak, J.K.; Kedare, S.B. Comparision of line focusing solar concentrator fields considering shading and blocking. *Sol. Energy* **2015**, *122*, 924–939. [CrossRef]
21. Onubogu, N.O.; Chong, K.-K.; Wong, C.-W.; Yew, T.-K.; Lim, B.-H. Optical characterization of two-stage non-imaging solar concentrator for active daylighting system. *Sol. Energy* **2019**, *185*, 24–33. [CrossRef]
22. Xiao, J.; Wei, X.; Gilaber, R.N.; Zhang, Y.; Li, Z. Design and characterization of a high-flux non-coaxial concentrating solar simulator. *Appl. Therm. Eng.* **2018**, *145*, 201–211. [CrossRef]

23. Barbon, A.; Barbón, N.; Bayón, L.; Otero, J. Theoretical elements for the design of a small scale Linear Fresnel Reflector: Frontal and lateral views. *Sol. Energy* **2016**, *132*, 188–202. [CrossRef]
24. Boito, P.; Grena, R. Optimizaition of the geometry of Fresnel linear collectors. *Sol. Energy* **2016**, *135*, 479–486. [CrossRef]
25. Zhu, Y.; Shi, J.; Li, Y.; Wang, L.; Huang, Q.; Xu, G. Design and experimental investigation of a stretched parabolic linear Fresnel reflector collecting system. *Energy Convers. Manag.* **2016**, *126*, 89–98. [CrossRef]
26. N'Tsoukpoe, K.E.; Azoumah, K.Y.; Ramde, E.; Fiagbe, A.Y.; Neveu, P.; Py, X.; Gaye, M.; Jourdan, A. Integrated design and construction of a micro-central tower power plant. *Energy Sustain. Dev.* **2016**, *31*, 1–13. [CrossRef]
27. Loni, R.; Kasaeian, A.; Asli-Ardeh, E.A.; Ghobadian, B. Optimizing the efficiency of a solar receiver with tubular cylindrical cavity for a solar-powered organic Rankine cycle. *Energy* **2016**, *112*, 1259–1272. [CrossRef]
28. Liang, C.-W.; Lin, J.-S. High concentration thin profile solar concentrator utilizing toroidal confocal relay. *Sol. Energy* **2015**, *122*, 264–270. [CrossRef]
29. Dähler, F.; Ambrosetti, G.; Montoya-Zegarra, J.A.; Schindler, K.; Steinfeld, A. High-concentration solar dishes based on pneumatic reflecting membranes. *Sol. Energy* **2016**, *124*, 89–100. [CrossRef]
30. Canavarro, D.; Chaves, J.; Collares-Pereira, M. A novel Compound Elliptical-type Concentrator for parabolic primaries with tubular receiver. *Sol. Energy* **2016**, *134*, 383–391. [CrossRef]
31. Tsai, C.-Y. Improved irradiance distribution on high concentration solar cell using free-form concentrator. *Sol. Energy* **2015**, *115*, 694–707. [CrossRef]
32. Tsai, C.-Y. Optimized solar thermal concentrator system based on free-form trough reflector. *Sol. Energy* **2016**, *125*, 146–160. [CrossRef]
33. Perez-Enciso, R.; Gallo, A.; Riveros-Rosas, D.; Fuentealba-Vidal, E.; Perez-Rábago, C. A simple method to achieve a uniform flux distribution in a multi-faceted point focus concentrator. *Renew. Energy* **2016**, *93*, 115–124. [CrossRef]
34. Meng, X.-L.; Xia, X.-L.; Sun, C.; Li, Y.; Li, X.-L. A novel free-form Cassegrain concentrator for PV/T combining utilization. *Sol. Energy* **2016**, *135*, 864–873. [CrossRef]
35. Shanks, K.; Ferrer-Rodriguez, J.P.; Fernández, E.F.; Almonacid, F.; Pérez-Higueras, P.; Senthilarasu, S.; Mallick, T. A >3000 suns high concentrator photovoltaic design based on multiple Fresnel lens primaries focusing to one central solar cell. *Sol. Energy* **2018**, *169*, 457–467. [CrossRef]
36. Wang, G.; Wang, F.; Shen, F.; Jiang, T.; Chen, Z.; Hu, P. Experimental and optical performances of a solar CPV device using a linear Fresnel reflector concentrator. *Renew. Energy* **2020**, *146*, 2351–2361. [CrossRef]
37. Zheng, H.; Feng, C.; Su, Y.; Dai, J.; Ma, X. Design and experimental analysis of a cylindrical compound Fresnel solar concentrator. *Sol. Energy* **2014**, *107*, 26–37. [CrossRef]
38. Sahin, F.E.; Yılmaz, M. High Concentration Photovoltaics (HCPV) with Diffractive Secondary Optical Elements. *Photonics* **2019**, *6*, 68. [CrossRef]
39. Qin, H.; Pang, X. Novel method to design laser beam shaping lenses using PSO techniques. *Appl. Phys. B* **2019**, *125*, 7. [CrossRef]
40. Pang, X.; Qin, H. Method for employing particle swarm algorithm to design LED collimator system. *J. Optoelectron. Adv. Mater.* **2019**, *21*, 35–47.
41. Qin, H. Aberration correction of a single aspheric lens with particle swarm algorithm. *Opt. Commun.* **2012**, *285*, 2996–3000. [CrossRef]
42. García-Botella, A.; Jiang, L.; Winston, R. Flowline Optical Simulation to Refractive/Reflective 3D Systems: Optical Path Length Correction. *Photonics* **2019**, *6*, 101. [CrossRef]
43. Sahin, F.E. Open-source optimization algorithms for optical design. *Optik* **2019**, *178*, 1016–1022. [CrossRef]
44. Houllier, T.; Lépine, T. Comparing optimization algorithms for conventional and freeform optical design: Erratum. *Opt. Express* **2019**, *27*, 28383. [CrossRef]